AIMS Mathematics, 10(6): 14596–14616.
DOI: 10.3934/math.2025657
Received: 01 May 2025
Revised: 12 June 2025
Accepted: 16 June 2025
Published: 26 June 2025

https://www.aimspress.com/journal/Math

Research article

Analytical study of the nonlinear dynamical systems: Application of the neural networks method

Jan Muhammad[1], Ghulam Hussain Tipu[1], Yasser Alrashedi[2], Mofareh Alhazmi[3] and Usman Younas[1,*]

[1] Department of Mathematics, Shanghai University, Shanghai 200444, China
[2] Department of Mathematics, College of Science, Taibah University, P.O. Box 344, Madinah 42353, Saudi Arabia
[3] Mathematics Department, College of Science, Jouf University, P.O. Box 2014, Sakaka, Saudi Arabia

* **Correspondence:** Email: usmanalgebra@shu.edu.cn.

Abstract: In this paper, we study the numerous complex dynamics of the nonlinear partial differential equations, namely the nonlinear Murray equation and nano-ionic currents along microtubules dynamical equations. Research has focused on solitary wave solutions because they provide important insights into nonlinear processes and have a variety of practical applications. Their exceptional behaviours and reliability represent creative nonlinear models across numerous fields, including physical, biological, and medical modeling. This research introduces Riccati subequation neural networks to derive exact solutions for space-time partial differential equations. The suggested technique integrates the solutions of the Riccati problem into neural networks. Neural networks are multi-layer computational representations consisting of activation and weights functions connecting neurons across input, hidden, and output layers. In this method, each neuron in the first hidden layer is allocated to the solutions of the Riccati equation. Thus, the new trial functions are derived. The suggested approach provides exact solutions of space-time partial differential equations. To validate the mathematical framework of this technique, we examine the proposed equations, resulting in the derivation of generalized hyperbolic function solutions, generalized trigonometric function solutions, and generalized rational solutions. This research presents novel solutions, as the presented approach is applied to the neural networks model for the first time. The dynamic properties of some solutions related to waves are shown using various graphics. This study advances knowledge of nonlinear dynamics in specific systems by demonstrating the method's efficacy.

Keywords: Riccati subequation neural networks; nonlinear equations; solitons
Mathematics Subject Classification: 35C07, 35C08, 35C15

1. Introduction

In today's technological era, the study of nonlinear wave dynamics has gained increasing attention among researchers. In many scientific fields, nonlinear partial differential equations (NLPDEs) [1] are crucial for understanding nonlinear wave phenomena in numerous nonlinear problems arising in various physical and industrial systems. NLPDEs have garnered a lot of attention in the nonlinear sciences due to their many applications. Numerous scholars are attempting to develop novel methods for solving NLPDEs in light of its numerous applications. In a wide range of fields, such as ocean engineering, biology, geology, quantum physics, optical fibers, plasma physics, and fluid mechanics, NLPDEs are regarded as an essential tool for characterizing nonlinear situations [2–5]. NLPDEs are important mathematical tools for representing the spatial and temporal development of complex behaviours including pattern development, turbulence, and abrupt transitions by considering the interactions of complex variables. In fluid dynamics, the Navier-Stokes equations' nonlinear components explain how air or water currents interact with one another to produce the chaotic flows and vortices required for weather forecasting. Diffusion-reaction PDEs forecast the electrical and diffuse propagation of nerve impulses or the patterns of animal coats caused by chemical gradients (morphogens). Nonlinear science's versatility is shown by its vast range of applications, from weather forecasting and optical networking to biological processes and financial modelling. Since nonlinear science has the fundamental principles governing self-organization, stability, and issues, it is essential to theoretical and technological development. The use of nonlinear techniques to stability, bifurcations, and natural phenomena may improve the prediction and control of many systems. Finding common ground across seemingly unrelated domains of inquiry is the goal of nonlinear research. This approach significantly improves our capacity to understand and handle complex, interrelated problems in the fields of technology and the natural sciences.

Neural networks have replaced analytical and numerical methods for solving NLPDEs due to their ability to solve complex, high-dimensional problems without discretization or solvability limits. They can express complicated nonlinear relationships without assumptions and can solve NLPDEs and infer the inverse case of unknown parameters. Despite challenges with stability and generalization, their ability to handle irregular domains, adaptive refinement, and parallel computation make them a versatile and scalable approach to scientific machine learning. Their combination with known methods has advanced computational mathematics and engineering. Neural networks have transformed several sectors, such as computer vision, natural language processing, generative adversarial networks, reinforcement learning systems, banking, healthcare, and voice recognition. They can help forecast market patterns, identify fraud, and help with drug discovery. Despite issues like processing costs and interpretability, neural networks are fundamental to modern artificial intelligence as they automate complexity and extract insights from large, dynamic data sets, revolutionizing sectors like voice recognition, recommendation systems, and climate modeling.

Nonlinear waves that maintain their shape while moving are called solitary waves. Unlike solutions to linear PDEs, which need a complicated balance between nonlinearity and dispersion, integrated soliton solutions to diverse NLPDEs may propagate over extended distances without dispersion [6]. Solitons exist in optics, fluid dynamics, and quantum domains, therefore NLPDEs are essential for modelling ocean waves or optical fiber pulse transmission. The integrability of certain NLPDEs allows analytical soliton solutions using the inverse scattering transform, providing fundamental insights into

wave dynamics. Beyond integrable systems, NLPDEs exhibit approximate soliton-like structures in increasingly complex contexts, highlighting their importance in theory and practice. To advance soliton theory and its applications in other domains, NLPDEs research is essential for numerous nonlinear phenomena.

Fundamental properties can be ascertained by deriving exact solutions for various physical processes. These methodologies provide a basis for further study, underscoring their significance. To acquire an exact solution, it is required to represent the fluctuations of the physical structure as an ODE or a PDE. PDEs may serve as mathematical models for intricate industrial and natural events. In recent decades, numerous methodologies have garnered significant attention to explore the nonlinear systems: Such as improved generalized exponential rational function approach [7], Adomian decomposition technique [8], truncated Painlevé technique [9], Lie symmetry approach [10], multivariate exponential rational integral function method [11], Riccati equation mapping approach [12], Darboux transformation [13], Bernoulli $\frac{G'}{G}$-expansion method [14], modified Sardar sub-equation technique [15], generalized Arnous approach [16], bifurcation analysis [17], fractional subequation neural network technique [18], and neural network for nonlinear problems [19–21], among others.

In this study, we apply the Riccati subequation neural network (RSENN) to solve NLPDEs such as nonlinear Murray equation and nano-ionic currents along microtubules dynamical equations, which is inspired by machine learning methods for solving PDEs and advancing the shortcomings of analytical methods. In this way, the solution of the Riccati equation is embedded in a neural network. The efficiency of the method used is crucial as well as the scope of their scientific and technological impact. The method used to analyze the data highlights important implications in order to achieve progress and propose viable alternatives in many scientific fields. We consider the RSENN method superior compared to the above mentioned methods, as it can be applied directly to obtain solutions of PDEs. In contrast, the other methods require converting the PDE into an ODE, which is not always feasible—especially when a suitable homogeneous balance number cannot be determined. In most cases, RSENN can be applied without such conversions, making it more versatile. The applied technique is very useful in a variety of situations due to the intricate relationship between nonlinearity and other factors while solving nonlinear problems.

The remaining sections of this article are organized as follows: Section 2 describes the Riccati subequation method, the neural networks model, the Riccati subequation neural networks and their graphical representation. Section 3 shows how the desired soliton solutions are computed applying the Riccati subequation neural networks of the proposed NLPDEs. A detailed explanation of the solutions' visual representation is given in Section 4. Section 5 provides concluding remarks.

2. Description of the Riccati subequation method

The key steps of the Riccati subequation method [22] for solving NLPDEs are summarized as follows. For any given PDE with variables $x,\ y,\ z$, and t

$$M\left(v, v_t, v_x, v_y, v_z, \frac{\partial v}{\partial t}, \frac{\partial v}{\partial x}, \frac{\partial v}{\partial y}, \frac{\partial v}{\partial z}, \ldots\right) = 0, \tag{2.1}$$

where $\frac{\partial v}{\partial t}, \frac{\partial v}{\partial x}, \frac{\partial v}{\partial y}, \frac{\partial v}{\partial z}$ are the partial derivatives of v with respect to $t,\ x,\ y,\ ,z$. The Riccati sub-equation method may be used to solve the ordinary differential equation $D\varphi(x) = \varpi + \varphi(x)^2$. The solutions of the proposed method are shown as follows:

Case-I: When $\varpi < 0$,

$$\begin{aligned}
\varphi_1(\xi) &= -\sqrt{-\varpi}\tanh(\sqrt{-\varpi}\xi),\\
\varphi_2(\xi) &= -\sqrt{-\varpi}\coth(\sqrt{-\varpi}\xi),\\
\varphi_3(\xi) &= -\sqrt{-\varpi}\tanh(2\sqrt{-\varpi}\xi) \pm i\sqrt{-\varpi}\,\mathrm{sech}(2\sqrt{-\varpi}\xi),\\
\varphi_4(\xi) &= -\sqrt{-\varpi}\coth(2\sqrt{-\varpi}\xi) \pm \sqrt{-\varpi}\,\mathrm{csch}(2\sqrt{-\varpi}\xi),\\
\varphi_5(\xi) &= -\frac{1}{2}\left(\sqrt{-\varpi}\tanh\left(\frac{\sqrt{-\varpi}}{2}\xi\right) + \sqrt{-\varpi}\coth\left(\frac{\sqrt{-\varpi}}{2}\xi\right)\right),\\
\varphi_6(\xi) &= \frac{\sqrt{-(\chi^2+\varrho^2)\varpi} - \chi\sqrt{-\varpi}\cosh(2\sqrt{-\varpi}\xi)}{\chi\sinh(2\sqrt{-\varpi}\xi) + \varrho},\\
\varphi_7(\xi) &= -\frac{\sqrt{-(\varrho^2-\chi^2)\varpi} - \chi\sqrt{-\varpi}\sinh(2\sqrt{-\varpi}\xi)}{\chi\cosh(2\sqrt{-\varpi}\xi) + \varrho}.
\end{aligned} \tag{2.2}$$

Case-II: When $\varpi > 0$,

$$\begin{aligned}
\varphi_8(\xi) &= \sqrt{\varpi}\tan(\sqrt{\varpi}\xi),\\
\varphi_9(\xi) &= -\sqrt{\varpi}\cot(\sqrt{\varpi}\xi),\\
\varphi_{10}(\xi) &= -\sqrt{\varpi}\tan(2\sqrt{\varpi}\xi) \pm \sqrt{\varpi}\sec(2\sqrt{\varpi}\xi),\\
\varphi_{11}(\xi) &= -\sqrt{\varpi}\cot(2\sqrt{\varpi}\xi) \pm \sqrt{\varpi}\csc(2\sqrt{\varpi}\xi),\\
\varphi_{12}(\xi) &= \frac{1}{2}\left(\sqrt{\varpi}\tan\left(\frac{\sqrt{\varpi}}{2}\xi\right) - \sqrt{\varpi}\cot\left(\frac{\sqrt{\varpi}}{2}\xi\right)\right),\\
\varphi_{13}(\xi) &= \frac{\pm\sqrt{(\chi^2-\varrho^2)\varpi} - \chi\sqrt{\varpi}\cos(2\sqrt{\varpi}\xi)}{\chi\sin(2\sqrt{\varpi}\xi) + \varrho},\\
\varphi_{14}(\xi) &= -\frac{\pm\sqrt{(\chi^2-\varrho^2)\varpi} - \chi\sqrt{\rho}\sin(2\sqrt{\varpi}\xi)}{\chi\cos(2\sqrt{\varpi}\xi) + \varrho},
\end{aligned} \tag{2.3}$$

where $\varrho,\ \chi$ are used with real numbers with $\chi^2 - \varrho^2 > 0$.

Case-III: When $\varpi = 0$,

$$\varphi_{15}(\xi) = -\frac{1}{\xi + m}, \tag{2.4}$$

where m is a constant.

2.1. Neural networks model

The trial function of the neural networks (NNs) model is introduced to determine the precise solutions of Eq (2.1). The solutions of Eq (2.1) are determined using the output of NNs as the trial function. Next, the trail function of the suggested method is described by

$$\Psi = W_{l_{n,\Psi}} F_{l_i}(\xi_{l_i}), \tag{2.5}$$

where the letter $W_{l_n,\Psi}$ represents the weight coefficient from the last hidden layer l_n to the output layer Ψ, F is the arbitrarily generalized activation function, and $l_n = \{I_{n-1}+1, I_{n-1}+2, \cdots, I_n\}$. The proposed neural network model has the following parameters Weights $W_{i,j}$ and bias term (b_l) from the (i)-th neuron of the preceding layer, which also form the output of the output layer. In the *lith* layer, the mathematical representation of ξ_{l_i} is described by

$$\xi_{l_i} = b_{l_i} + W_{l_{i-1},l_i} F_{l_{i-1}}\left(\xi_{l_{i-1}}\right), i = 1, 2, \ldots, n,$$

where

$$l_p = \{x, y, \ldots, t\}(p = 2, 3, \ldots, n-1).$$

The operational mechanism of the neural network model is executed by forward propagation, a process that transmits information from the input layer to the output layer, resulting in the final output via the weighted sum and activation function of neurons.

The neural network model is illustrated by Figure 1.

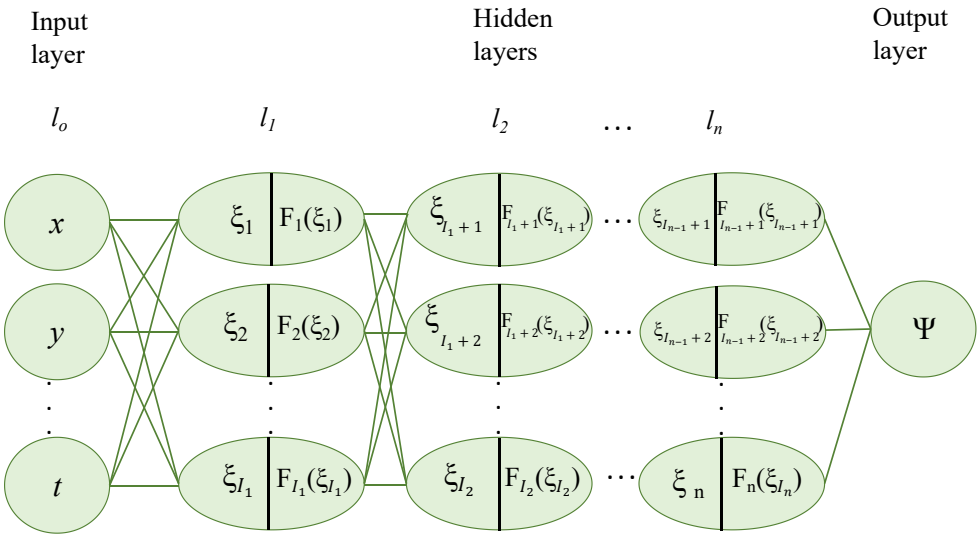

Figure 1. NNs model.

2.2. Riccati subequation neural networks

Riccati subequation neural networks (RSENNs) is new technique that combines the NNs model with the Riccati subequation method. There are two parts to the central concept of RSENNs. One advantage of NNs models is that the activation functions of the first hidden layer is derived from the solutions of Riccati subequation method. Further, it can be used as the trial function that will covert the PDE into algebraic expressions. The activation functions of the first hidden layer in the NNs model may be chosen as the solutions of the Riccati subequation when the Riccati subequation is coupled with NNs. This allows for the extraction of additional and novel exact solutions of PDEs. The key steps of the proposed method are the following:

Step-1: By using the Riccati subequation and activation functions of the first hidden layer on the NNs model, we may choose the Riccati equation as the desired equation.

Step-2: The RSENNs model can be built using the activation function of the first hidden layer chosen in Step 1. In this model, x, y, z, and t are input variables, and the selection of the subsequent hidden

layer can be done based on the circumstances. The output is then possible to obtain by means of feed-forward operation. Figure 2 provides a clear description of the NNs model.

Step-3: The trial functions of the solutions of PDEs may be obtained by using the forward propagation of the RSENNs model.

Step-4: To get the algebraic equations, we substitute the trial functions of RSENNs into the PDEs.

Step-5: We seek solutions to algebraic equations including variables like x, y, z, t, as well as the function $F(x, y, z, t), \cdots$. A set of algebraic equations may be derived by setting the coefficient of each term to zero for the equations developed in Step 4.

Step-6: Choose the most suitable coefficients solutions among all the possible coefficient solutions that satisfy the criteria after analyzing these algebraic equations. To find the first explicit solutions of Ψ, insert these values back into the trial function. An exact solution to Eq (2.1) may be found by using Eqs (2.2)–(2.4).

Assigning an appropriate number of neurons (Riccati subequation solutions) to the first hidden layer of the NNs model allows this approach to accomplish find more exact solutions, which is an obvious advantage.

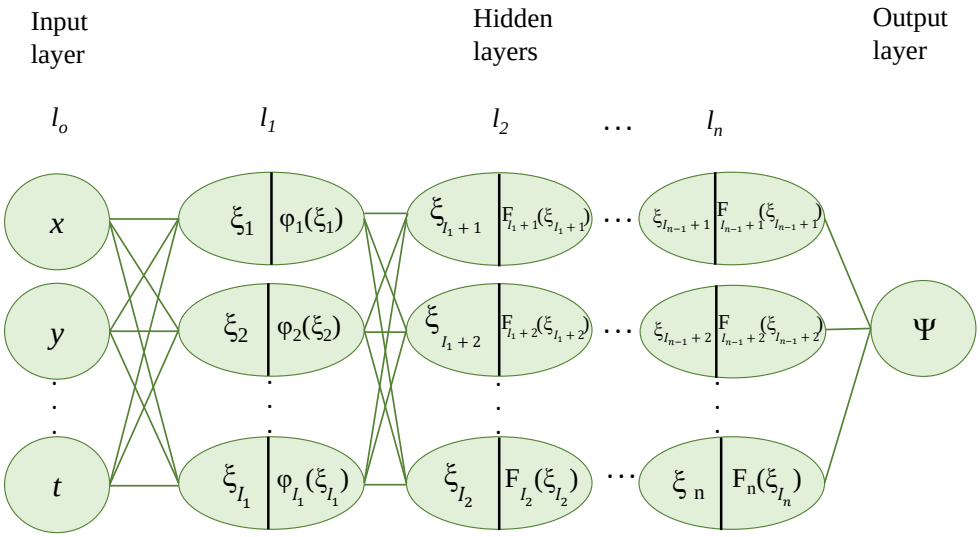

Figure 2. RSENNs model.

3. Applications

In this section, we will investigate two PDEs: the nonlinear Murray equation and nano-ionic currents along microtubules. We employ the 2-2-2-1 RSENNs model, which uses two neurons for each of the three layers (input, hidden, and output) and uses the trial function Ψ to find solutions to PDEs. We have

$$\Psi = b_5 + W_{3,\psi}F_3(\xi_3) + W_{4,\psi}F_4(\xi_4)^2, \tag{3.1}$$

where

$$\begin{cases} \xi_1 = b_1 + tW_{t,1} + xW_{x,1}, \\ \xi_2 = b_2 + tW_{t,2} + xW_{x,2}, \\ \xi_3 = b_3 + W_{1,3}F_1(\xi_1) + W_{2,3}F_2(\xi_2), \\ \xi_4 = b_4 + W_{1,4}F_1(\xi_1) + W_{2,4}F_2(\xi_2), \end{cases} \tag{3.2}$$

where F_i with $(i = 1, 2, 3, 4)$ denotes the activation function, b_l with $(l = 1, 2, 3, 4, 5)$, and $W_{j,k}(j = x, t, 1, 2, 3, 4,\ k = 1, 2, 3, 4, \Psi, j \neq k)$ are used to denote the real parameters to be determined later.

Here, we use the 2-2-2-1 RSENNs model for the sake of simplicity. The first hidden layer's activation functions are the solutions of the Riccati equation $\varphi()$, and the second layer's activation functions are the identity function $(\cdot)$ and the square function $(\cdot)^2$, and hence, the inputs are x and t. The following is the output of these NNs, which is used as the trial function of PDEs:

$$\Psi = b_5 + W_{3,\psi}(\xi_3) + W_{4,\psi}(\xi_4)^2, \tag{3.3}$$

where

$$\begin{cases} \xi_1 = b_1 + tW_{t,1} + xW_{x,1}, \\ \xi_2 = b_2 + tW_{t,2} + xW_{x,2}, \\ \xi_3 = b_3 + W_{1,3}\varphi(\xi_1) + W_{2,3}\varphi(\xi_2), \\ \xi_4 = b_4 + W_{1,4}\varphi(\xi_1) + W_{2,4}\varphi(\xi_2). \end{cases} \tag{3.4}$$

Figure 3 provides a simple explanation of the 2-2-2-1 RSENNs model. Let $b_i = 0$ for $i = 1, 2, 3, 4$ and set $b_5 = b$ in the actual computation to simplify the calculation. Hence, the 2-2-2-1 RSENNs model's formula reads:

$$\begin{aligned} \Psi =& b + W_{3,\Psi}\left(W_{1,3}\varphi\left(tW_{t,1} + xW_{x,1}\right) + W_{2,3}\varphi\left(tW_{t,2} + xW_{x,2}\right)\right) \\ &+ W_{4,\Psi}\left(W_{1,4}\varphi\left(tW_{t,1} + xW_{x,1}\right) + W_{2,4}\varphi\left(tW_{t,2} + xW_{x,2}\right)\right)^2. \end{aligned} \tag{3.5}$$

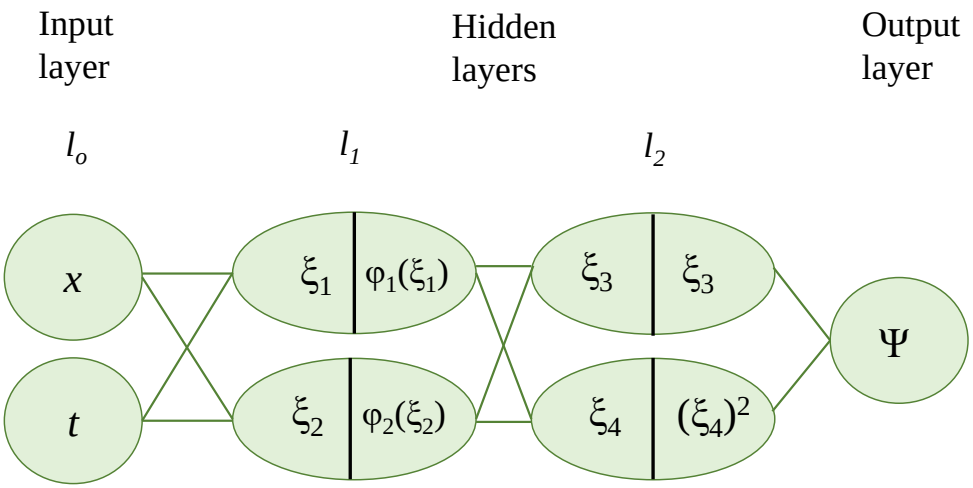

Figure 3. 2-2-2-1 RSENNs model of Eq (3.3).

3.1. Nonlinear Murray equation

In this subsection, we calculate the desired solutions for the nonlinear Murray equation. The proposed equation is an important concept in medical theory, known as Murray's law or principle, explains how the diameter of an artery affects the rate of blood flow. The nonlinear Murray equation serves as mathematical model that takes into account, among other things, the impact of fluid dynamics and blood flow geometry, and is described by:

$$R^3 = C_1\left(\frac{Q}{w}\right)^2 + D_1\left(\frac{w}{L}\right), \tag{3.6}$$

whereas L represents the vessel's length, and the parameters w, C_1, and D_1 are real constants. The flow rate of blood through the vessel is denoted by Q, while the blood vessel radius is represented by the letter R. The convection term is incorporated into the nonlinear reaction-diffusion equation [23, 24], which is presented as follows:

$$\Psi_t = A(\Psi)\Psi_{xx} + B(\Psi)\Psi_x + C_2(\Psi), \tag{3.7}$$

where $\Psi = \Psi(x,t)$ is unknown and $A(\Psi)$, $B(\Psi)$, $C_2(\Psi)$ are chosen as arbitrary smooth functions. Taking $A(\Psi) = 1$, $B(\Psi) = G\Psi$ and $C_2(\Psi) = H\Psi - K\Psi^2$, then Eq (3.7) reads [25, 26] as:

$$\Psi_t - \Psi_{xx} - G\Psi\Psi_x - H\Psi + K\Psi^2 = 0, \tag{3.8}$$

where the parameters G, H, K are determined later. By substituting Eq (3.5) in Eq (3.8) and simplifying the results, we obtain the following solutions:

Case-I: When $\varpi < 0$, and $W_{1,4} = 0$, $W_{1,3} = -\frac{2W_{x,1}}{GW_{3,\Psi}}$, $W_{2,3} = 0$, $W_{2,4} = 0$, $b = \frac{2\sqrt{-\varpi}W_{x,1}}{G}$, $H = 4\varpi W_{x,1}^2 + 2\sqrt{-\varpi}W_{t,1}$, $K = \frac{GW_{t,1}}{2W_{x,1}} - G\sqrt{-\varpi}W_{x,1}$. The soliton solutions are calculated as follows:

The kink-type soliton solution:

$$\Psi_{1.1}(x,t) = \frac{2\sqrt{-\varpi}W_{x,1}\tanh\left(\sqrt{-\varpi}\left(tW_{t,1} + xW_{x,1}\right)\right)}{G} + \frac{2\sqrt{-\varpi}W_{x,1}}{G}. \tag{3.9}$$

The singular soliton solution:

$$\Psi_{1.2}(x,t) = \frac{2\sqrt{-\varpi}W_{x,1}\coth\left(\sqrt{-\varpi}\left(tW_{t,1} + xW_{x,1}\right)\right)}{G} + \frac{2\sqrt{-\varpi}W_{x,1}}{G}. \tag{3.10}$$

Bright-dark soliton solution:

$$\Psi_{1.3}(x,t) = \frac{2\sqrt{-\varpi}W_{x,1}\left(\tanh\left(2\sqrt{-\varpi}\left(tW_{t,1} + xW_{x,1}\right)\right) + i\,\mathrm{sech}\left(2\sqrt{-\varpi}\left(tW_{t,1} + xW_{x,1}\right)\right)\right)}{G} + \frac{2\sqrt{-\varpi}W_{x,1}}{G}. \tag{3.11}$$

The soliton solution:

$$\Psi_{1.4}(x,t) = \frac{2\sqrt{-\varpi}W_{x,1}\left(\coth\left(2\sqrt{-\varpi}\left(tW_{t,1} + xW_{x,1}\right)\right) + \mathrm{csch}\left(2\sqrt{-\varpi}\left(tW_{t,1} + xW_{x,1}\right)\right)\right)}{G} + \frac{2\sqrt{-\varpi}W_{x,1}}{G}. \tag{3.12}$$

When $W_{1,3} = -\frac{2W_{x,1}}{GW_{3,\Psi}}$, $W_{2,3} = 0$, $b = \frac{2\sqrt{-\varpi}W_{x,1}}{G}$, $W_{4,\Psi} = 0$, $H = 4\varpi W_{x,1}^2 + 2\sqrt{-\varpi}W_{t,1}$, $K = \frac{GW_{t,1}}{2W_{x,1}} - G\sqrt{-\varpi}W_{x,1}$, we obtain the solutions as follows:

The soliton solution:

$$\Psi_{1.5}(x,t) = -\frac{W_{x,1}\left(\sqrt{-\varpi}\left(-\tanh\left(\frac{1}{2}\sqrt{-\varpi}\left(tW_{t,1} + xW_{x,1}\right)\right)\right) + \left(-\sqrt{-\varpi}\right)\coth\left(\frac{1}{2}\sqrt{-\varpi}\left(tW_{t,1} + xW_{x,1}\right)\right)\right)}{G} + \frac{2\sqrt{-\varpi}W_{x,1}}{G}. \tag{3.13}$$

The singular soliton solutions:

$$\Psi_{1.6}(x,t) = -\frac{2W_{x,1}\left(\sqrt{-\varpi\left(\chi^2 + \varrho^2\right)} - \chi\sqrt{-\varpi}\cosh\left(2\sqrt{-\varpi}\left(tW_{t,1} + xW_{x,1}\right)\right)\right)}{G\left(\chi\sinh\left(2\sqrt{-\varpi}\left(tW_{t,1} + xW_{x,1}\right)\right) + \varrho\right)} + \frac{2\sqrt{-\varpi}W_{x,1}}{G}, \tag{3.14}$$

$$\Psi_{1.7}(x,t) = -\frac{2W_{x,1}\left(\sqrt{-\varpi\left(\varrho^2-\chi^2\right)}-\chi\sqrt{-\varpi}\sinh\left(2\sqrt{-\varpi}\left(tW_{t,1}+xW_{x,1}\right)\right)\right)}{G\left(\chi\cosh\left(2\sqrt{-\varpi}\left(tW_{t,1}+xW_{x,1}\right)\right)+\varrho\right)}+\frac{2\sqrt{-\varpi}W_{x,1}}{G}. \quad (3.15)$$

Case-II: When $\varpi > 0$, and $W_{1,4} = 0$, $W_{1,3} = -\frac{2W_{x,1}}{GW_{3,\Psi}}$, $W_{2,3} = 0$, $W_{2,4} = 0$, $b = \frac{2i\sqrt{\varpi}W_{x,1}}{G}$, $H = 4\varpi W_{x,1}^2 + 2i\sqrt{\varpi}W_{t,1}$, $K = \frac{GW_{t,1}}{2W_{x,1}} - iG\sqrt{\varpi}W_{x,1}$. The periodic soliton solutions are calculated as follows:

$$\Psi_{1.8}(x,t) = -\frac{2\sqrt{\varpi}W_{x,1}\tan\left(\sqrt{\varpi}\left(tW_{t,1}+xW_{x,1}\right)\right)}{G}+\frac{2i\sqrt{\varpi}W_{x,1}}{G}, \quad (3.16)$$

$$\Psi_{1.9}(x,t) = \frac{2\sqrt{\varpi}W_{x,1}\cot\left(\sqrt{\varpi}\left(tW_{t,1}+xW_{x,1}\right)\right)}{G}+\frac{2i\sqrt{\varpi}W_{x,1}}{G}, \quad (3.17)$$

$$\Psi_{1.10}(x,t) = -\frac{2\sqrt{\varpi}W_{x,1}\left(\tan\left(2\sqrt{\varpi}\left(tW_{t,1}+xW_{x,1}\right)\right)+\sec\left(2\sqrt{\varpi}\left(tW_{t,1}+xW_{x,1}\right)\right)\right)}{G}+\frac{2i\sqrt{\varpi}W_{x,1}}{G}, \quad (3.18)$$

$$\Psi_{1.11}(x,t) = \frac{2\sqrt{\varpi}W_{x,1}\left(\cot\left(2\sqrt{\varpi}\left(tW_{t,1}+xW_{x,1}\right)\right)+\csc\left(2\sqrt{\varpi}\left(tW_{t,1}+xW_{x,1}\right)\right)\right)}{G}+\frac{2i\sqrt{\varpi}W_{x,1}}{G}. \quad (3.19)$$

When $W_{1,3} = -\frac{2W_{x,1}}{GW_{3,\Psi}}$, $W_{2,3} = 0$, $b = \frac{2i\sqrt{\varpi}W_{x,1}}{G}$, $W_{4,\Psi} = 0$, $H = 4\varpi W_{x,1}^2 + 2i\sqrt{\varpi}W_{t,1}$, $K = \frac{GW_{t,1}}{2W_{x,1}} - iG\sqrt{\varpi}W_{x,1}$, we obtain the periodic solutions as follows:

$$\Psi_{1.12}(x,t) = -\frac{W_{x,1}\left(\sqrt{\varpi}\tan\left(\frac{1}{2}\sqrt{\varpi}\left(tW_{t,1}+xW_{x,1}\right)\right)-\sqrt{\varpi}\cot\left(\frac{1}{2}\sqrt{\varpi}\left(tW_{t,1}+xW_{x,1}\right)\right)\right)}{G}+\frac{2i\sqrt{\varpi}W_{x,1}}{G}, \quad (3.20)$$

$$\Psi_{1.13}(x,t) = -\frac{2W_{x,1}\left(\sqrt{\varpi\left(\chi^2-\varrho^2\right)}-\chi\sqrt{\varpi}\cos\left(2\sqrt{\varpi}\left(tW_{t,1}+xW_{x,1}\right)\right)\right)}{G\left(\chi\sin\left(2\sqrt{\varpi}\left(tW_{t,1}+xW_{x,1}\right)\right)+\varrho\right)}+\frac{2i\sqrt{\varpi}W_{x,1}}{G}, \quad (3.21)$$

$$\Psi_{1.14}(x,t) = \frac{2W_{x,1}\left(\sqrt{\varpi\left(\chi^2-\varrho^2\right)}-\chi\sqrt{\varpi}\sin\left(2\sqrt{\varpi}\left(tW_{t,1}+xW_{x,1}\right)\right)\right)}{G\left(\chi\cos\left(2\sqrt{\varpi}\left(tW_{t,1}+xW_{x,1}\right)\right)+\varrho\right)}+\frac{2i\sqrt{\varpi}W_{x,1}}{G}, \quad (3.22)$$

where ϱ, χ are used to represent real numbers with $\chi^2 - \varrho^2 > 0$.

3.2. Nano-ionic currents along microtubules dynamical equations

Microtubules (MTs), the most important part of each cell's structure, are cylindrical polymers derived from tubulin. The functional role of MTs is determined by their ability to transition across a wide range of sizes [27]. The transport and movement of cells are aided by the 13 parallel

protofilaments that comprise MTs [28]. The transmission line models of nano ionic currents along MTs [29, 30] are as follows:

$$\alpha\Psi_{xxx} + \gamma\Psi\Psi_t + 2\Psi_x + \lambda\Psi_t + \theta\Psi = 0, \tag{3.23}$$

where $\Psi = \Psi(x,t)$ represents the complex wave profile, and parameters $\alpha,\ \gamma,\ \lambda,\ \theta$ are determined later. By substituting Eq (3.5) in Eq (3.23) and simplifying the results, we obtain the solutions as follows:

Case-I: When $\varpi < 0$, and $W_{1,4} = 0,\ W_{1,3} = 0,\ W_{2,3} = 0,\ W_{t,2} = -\frac{12\alpha W_{x,2}^3}{\gamma W_{2,4}^2 W_{4,\Psi}},\ \lambda = \frac{\gamma W_{2,4}^2 W_{4,\Psi}\left(4\alpha\varpi W_{x,2}^2+1\right)}{6\alpha W_{x,2}^2} - b\gamma,\ \theta = 0$. The soliton solutions are calculated as follows:

The dark soliton solution:

$$\Psi_{2.1}(x,t) = -\varpi W_{2,4}^2 W_{4,\Psi}\tanh^2\left(\sqrt{-\varpi}\left(xW_{x,2} - \frac{12\alpha t W_{x,2}^3}{\gamma W_{2,4}^2 W_{4,\Psi}}\right)\right). \tag{3.24}$$

The singular soliton solution:

$$\Psi_{2.2}(x,t) = b - \varpi W_{2,4}^2 W_{4,\Psi}\coth^2\left(\sqrt{-\varpi}\left(xW_{x,2} - \frac{12\alpha t W_{x,2}^3}{\gamma W_{2,4}^2 W_{4,\Psi}}\right)\right). \tag{3.25}$$

The bright-dark soliton solution:

$$\Psi_{2.3}(x,t) = b - \varpi W_{2,4}^2 W_{4,\Psi}\left(\tanh\left(2\sqrt{-\varpi}\left(xW_{x,2} - \frac{12\alpha t W_{x,2}^3}{\gamma W_{2,4}^2 W_{4,\Psi}}\right)\right) + i\,\mathrm{sech}\left(2\sqrt{-\varpi}\left(xW_{x,2} - \frac{12\alpha t W_{x,2}^3}{\gamma W_{2,4}^2 W_{4,\Psi}}\right)\right)\right)^2. \tag{3.26}$$

The soliton solution:

$$\Psi_{2.4}(x,t) = b - \varpi W_{2,4}^2 W_{4,\Psi}\left(\coth\left(2\sqrt{-\varpi}\left(xW_{x,2} - \frac{12\alpha t W_{x,2}^3}{\gamma W_{2,4}^2 W_{4,\Psi}}\right)\right) + \mathrm{csch}\left(2\sqrt{-\varpi}\left(xW_{x,2} - \frac{12\alpha t W_{x,2}^3}{\gamma W_{2,4}^2 W_{4,\Psi}}\right)\right)\right)^2. \tag{3.27}$$

When $W_{1,3} = 0,\ W_{2,3} = 0,\ W_{2,4} = 0,\ W_{t,1} = -\frac{12\alpha W_{x,1}^3}{\gamma W_{1,4}^2 W_{4,\Psi}},\ W_{x,2} = 0,\ \lambda = \frac{\gamma W_{1,4}^2 W_{4,\Psi}\left(4\alpha\varpi W_{x,1}^2+1\right)}{6\alpha W_{x,1}^2},\ b = 0,\ \theta = 0$, we get solutions:

The dark-singular soliton solution:

$$\Psi_{2.5}(x,t) = \frac{1}{4}W_{1,4}^2 W_{4,\Psi}\left(\sqrt{-\varpi}\left(-\tanh\left(\frac{1}{2}\sqrt{-\varpi}\left(xW_{x,1} - \frac{12\alpha t W_{x,1}^3}{\gamma W_{1,4}^2 W_{4,\Psi}}\right)\right)\right)\right.$$
$$\left. + \left(-\sqrt{-\varpi}\right)\coth\left(\frac{1}{2}\sqrt{-\varpi}\left(xW_{x,1} - \frac{12\alpha t W_{x,1}^3}{\gamma W_{1,4}^2 W_{4,\Psi}}\right)\right)\right)^2. \tag{3.28}$$

The singular soliton solutions:

$$\Psi_{2.6}(x,t) = \frac{W_{1,4}^2 W_{4,\Psi}\left(\sqrt{-\varpi\left(\chi^2+\varrho^2\right)} - \chi\sqrt{-\varpi}\cosh\left(2\sqrt{-\varpi}\left(xW_{x,1} - \frac{12\alpha t W_{x,1}^3}{\gamma W_{1,4}^2 W_{4,\Psi}}\right)\right)\right)^2}{\left(\chi\sinh\left(2\sqrt{-\varpi}\left(xW_{x,1} - \frac{12\alpha t W_{x,1}^3}{\gamma W_{1,4}^2 W_{4,\Psi}}\right)\right) + \varrho\right)^2}, \tag{3.29}$$

$$\Psi_{2.7}(x,t)=\frac{W_{1,4}^2W_{4,\Psi}\left(\sqrt{-\varpi\left(\varrho^2-\chi^2\right)}-\chi\sqrt{-\varpi}\sinh\left(2\sqrt{-\varpi}\left(xW_{x,1}-\frac{12\alpha tW_{x,1}^3}{\gamma W_{1,4}^2W_{4,\Psi}}\right)\right)\right)^2}{\left(\chi\cosh\left(2\sqrt{-\varpi}\left(xW_{x,1}-\frac{12\alpha tW_{x,1}^3}{\gamma W_{1,4}^2W_{4,\Psi}}\right)\right)+\varrho\right)^2}. \tag{3.30}$$

Case-II: When $\varpi > 0$, and $W_{1,4}=0,\ W_{1,3}=0,\ W_{2,3}=0,\ W_{t,2}=-\frac{12\alpha W_{x,2}^3}{\gamma W_{2,4}^2W_{4,\Psi}},\ \lambda=\frac{\gamma W_{2,4}^2W_{4,\Psi}\left(4\alpha\varpi W_{x,2}^2+1\right)}{6\alpha W_{x,2}^2}-b\gamma,\ \theta=0$. The periodic soliton solutions are calculated as:

$$\Psi_{2.8}(x,t)=\varpi W_{2,4}^2W_{4,\Psi}\tan^2\left(\sqrt{\varpi}\left(xW_{x,2}-\frac{12\alpha tW_{x,2}^3}{\gamma W_{2,4}^2W_{4,\Psi}}\right)\right)+b, \tag{3.31}$$

$$\Psi_{2.9}(x,t)=\varpi W_{2,4}^2W_{4,\Psi}\cot^2\left(\sqrt{\varpi}\left(xW_{x,2}-\frac{12\alpha tW_{x,2}^3}{\gamma W_{2,4}^2W_{4,\Psi}}\right)\right)+b, \tag{3.32}$$

$$\Psi_{2.10}(x,t)=\varpi W_{2,4}^2W_{4,\Psi}\left(\tan\left(2\sqrt{\varpi}\left(xW_{x,2}-\frac{12\alpha tW_{x,2}^3}{\gamma W_{2,4}^2W_{4,\Psi}}\right)\right)+\sec\left(2\sqrt{\varpi}\left(xW_{x,2}-\frac{12\alpha tW_{x,2}^3}{\gamma W_{2,4}^2W_{4,\Psi}}\right)\right)\right)^2+b, \tag{3.33}$$

$$\Psi_{2.11}(x,t)=\varpi W_{2,4}^2W_{4,\Psi}\left(\cot\left(2\sqrt{\varpi}\left(xW_{x,2}-\frac{12\alpha tW_{x,2}^3}{\gamma W_{2,4}^2W_{4,\Psi}}\right)\right)+\csc\left(2\sqrt{\varpi}\left(xW_{x,2}-\frac{12\alpha tW_{x,2}^3}{\gamma W_{2,4}^2W_{4,\Psi}}\right)\right)\right)^2+b. \tag{3.34}$$

When $W_{1,3}=0,\ W_{2,3}=0,\ W_{2,4}=0,\ W_{t,1}=-\frac{12\alpha W_{x,1}^3}{\gamma W_{1,4}^2W_{4,\Psi}},\ W_{x,2}=0,\ \lambda=\frac{\gamma W_{1,4}^2W_{4,\Psi}\left(4\alpha\varpi W_{x,1}^2+1\right)}{6\alpha W_{x,1}^2},\ b=0,\ \theta=0$, we obtain the periodic solutions as follows:

$$\Psi_{2.12}(x,t)=\frac{1}{4}W_{1,4}^2W_{4,\Psi}\left(\sqrt{\varpi}\tan\left(\frac{1}{2}\sqrt{\varpi}\left(xW_{x,1}-\frac{12\alpha tW_{x,1}^3}{\gamma W_{1,4}^2W_{4,\Psi}}\right)\right)-\sqrt{\varpi}\cot\left(\frac{1}{2}\sqrt{\varpi}\left(xw_{x,1}-\frac{12\alpha tW_{x,1}^3}{\gamma W_{1,4}^2W_{4,\Psi}}\right)\right)\right)^2, \tag{3.35}$$

$$\Psi_{2.13}(x,t)=\frac{W_{1,4}^2W_{4,\Psi}\left(\sqrt{\varpi\left(\chi^2-\varrho^2\right)}-\chi\sqrt{\varpi}\cos\left(2\sqrt{\varpi}\left(xW_{x,1}-\frac{12\alpha tW_{x,1}^3}{\gamma W_{1,4}^2W_{4,\Psi}}\right)\right)\right)^2}{\left(\chi\sin\left(2\sqrt{\varpi}\left(xW_{x,1}-\frac{12\alpha tW_{x,1}^3}{\gamma W_{1,4}^2W_{4,\Psi}}\right)\right)+\varrho\right)^2}, \tag{3.36}$$

$$\Psi_{2.14}(x,t)=\frac{W_{1,4}^2W_{4,\Psi}\left(\sqrt{\varpi\left(\chi^2-\varrho^2\right)}-\chi\sqrt{\varpi}\sin\left(2\sqrt{\varpi}\left(xW_{x,1}-\frac{12\alpha tW_{x,1}^3}{\gamma W_{1,4}^2W_{4,\Psi}}\right)\right)\right)^2}{\left(\chi\cos\left(2\sqrt{\varpi}\left(xW_{x,1}-\frac{12\alpha tW_{x,1}^3}{\gamma W_{1,4}^2W_{4,\Psi}}\right)\right)+\varrho\right)^2}, \tag{3.37}$$

where $\varrho,\ \chi$ are used to represent real numbers with $\chi^2-\varrho^2>0$.

4. Discussion and graphs

By meeting different analytical demands, 3D, 2D, and density graphs all play a significant role in data visualization. Although 3D graphs require careful interpretation to prevent perceptual distortions, they excel at depicting complicated, multidimensional data sets, therefore enabling researchers to observe interactions among three variables, such as spatial relationships in engineering, molecular structures in chemistry, or atmospheric patterns in meteorology. 2D graphs, such as line charts, scatter plots, or bar graphs, provide simplicity and clarity, making them perfect for showing trends, correlations, or comparisons over time or across categories, especially in sectors like economics, social sciences, and education, where clear communication is vital. Density graphs, like heatmaps or contour plots, draw attention to data concentration and distribution patterns, hence facilitating the detection of clusters, gradients, or anomalies in huge datasets. This is especially useful for population research, risk assessment, or machine learning. Taken together, these visualization tools offer complementary viewpoints: 2D graphs make data more accessible; 3D graphs provide depth for complex analysis; density graphs expose hidden structures; all three types of graphs improve decision-making, hypothesis testing, and narrative across scientific, industrial, and educational spheres. A variety of graphs are presented in Figures 4–12. Figure 4 has been sketched for the parametric values $\varpi = -0.02, W_{x,1} = 1.7, W_{t,1} = 0.2$, and $G = 2$ to the solution (3.9). The dynamics of the solution (3.11) has been plotted in Figures 5 and 6 by the assistance of the parametric values $\varpi = -0.02, W_{x,1} = 7, W_{t,1} = 2, G = 2$ and $\varpi = -0.05, W_{x,1} = 2.89, W_{t,1} = 2.5, G = 2.1$, respectively. Moreover, Figure 7 is depicted for the parameters $\varpi = -0.225, W_{x,1} = 1.2, W_{t,1} = 0.5, G = 5$ to the solution (3.13). Figure 8 is plotted to the solution (3.18) for the values $\varpi = 3.5, W_{x,1} = 0.6, W_{t,1} = 0.5, G = 0.2$. Furthermore, the parameters $\varpi = -0.02, W_{2,4} = 2, W_{4,\Psi} = 1.2, \gamma = 0.3, \alpha = 2.3, W_{x,2} = 0.05$ have been used for Figure 9 of the solution (3.24). Figures 10 and 11 have been plotted for the values $\varpi = -0.01, W_{2,4} = 2, W_{4,\Psi} = 2.2, \gamma = 1.3, \alpha = 0.03, W_{x,2} = 2.1, b = .1$ to the solution (3.26). Figure 12 is sketched for the values $\varpi = 0.06, W_{x,1} = 0.5, W_{2,4} = 0.2, W_{4,\Psi} = 0.002, \gamma = 3, \alpha = 0.3, W_{1,4} = 0.5, \chi = .2, \varrho = 0.1$ to the solution (3.37). A variety of shapes like kink, dark, bright, combined as well as the periodic solitary waves have been observed in the plotted figures. In nonlinear research and applied physics, kink, dark, bright, mixed, and periodic solitary waves are of great relevance because of their exceptional qualities and resilience in preserving shape and stability across great distances. Offering insights into symmetry-breaking events, kink waves (topological solitons) model phase transitions, domain walls in materials, or energy transmission in biological systems. While bright solitary waves (localized intensity peaks) allow consistent signal transmission in optical fibers and model self-trapped quantum states, dark solitary waves (intensity dips in nonlinear media) are essential in optics and Bose-Einstein condensates for controlling light pulses or investigating quantum superfluidity. Bridging localized and wavelike behaviours, periodic solitary waves such as cnoidal waves or soliton trains—describe repeated structures in oceanography, nonlinear optics, and transmission lines. These waves taken together support developments in photonics, quantum technologies, and atmospheric modelling by offering frameworks to govern energy, information, and matter in nonlinear environments vital for current communication systems, medical imaging, and fundamental physics research.

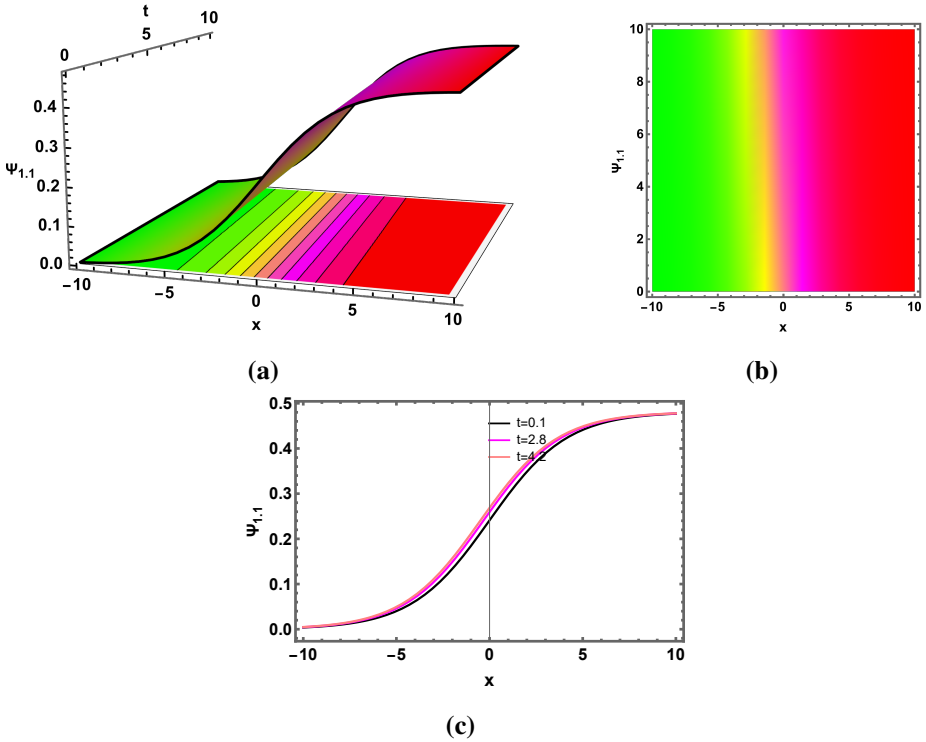

Figure 4. Dynamics of kink type solution (3.9) for the parameters $\varpi = -0.02, W_{x,1} = 1.7, W_{t,1} = 0.2$, and $G = 2$.

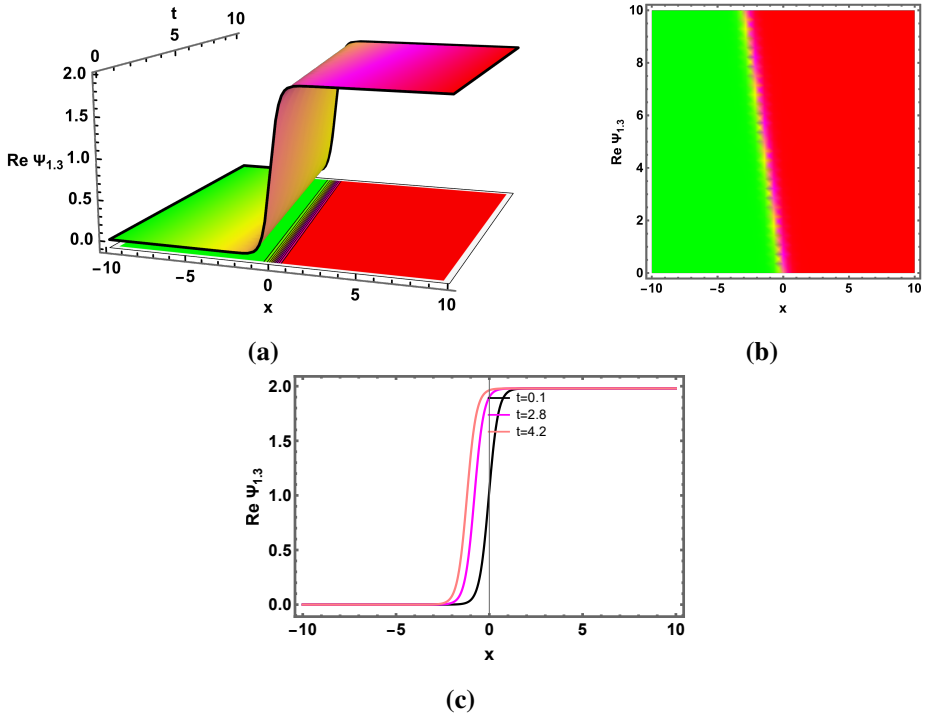

Figure 5. Dynamics of the real part of solution (3.11) for the parameters $\varpi = -0.02, W_{x,1} = 7, W_{t,1} = 2$, and $G = 2$.

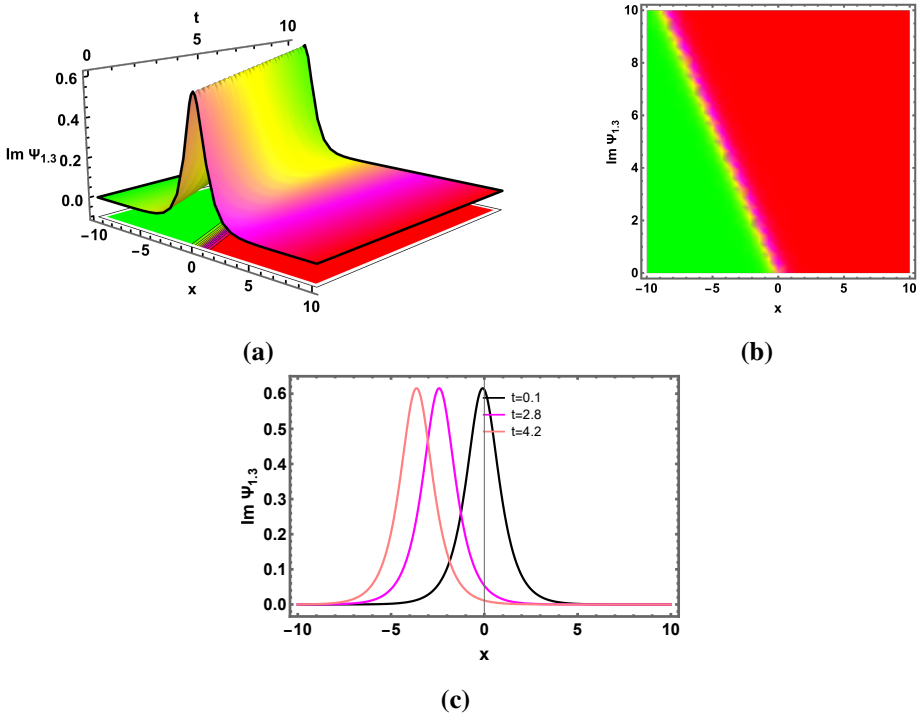

Figure 6. Dynamics of the imaginary part of solution (3.11) for the parameters $\varpi = -0.05$, $W_{x,1} = 2.89$, $W_{t,1} = 2.5$, and $G = 2.1$.

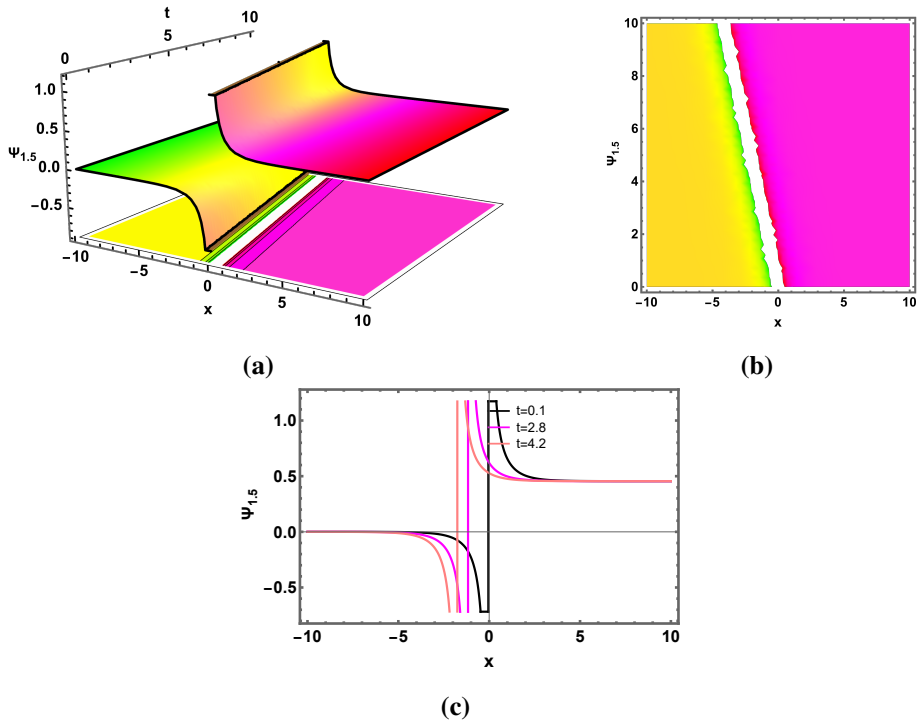

Figure 7. Dynamics of the soliton solution (3.13) for the parameters $\varpi = -0.225$, $W_{x,1} = 1.2$, $W_{t,1} = 0.5$, and $G = 5$.

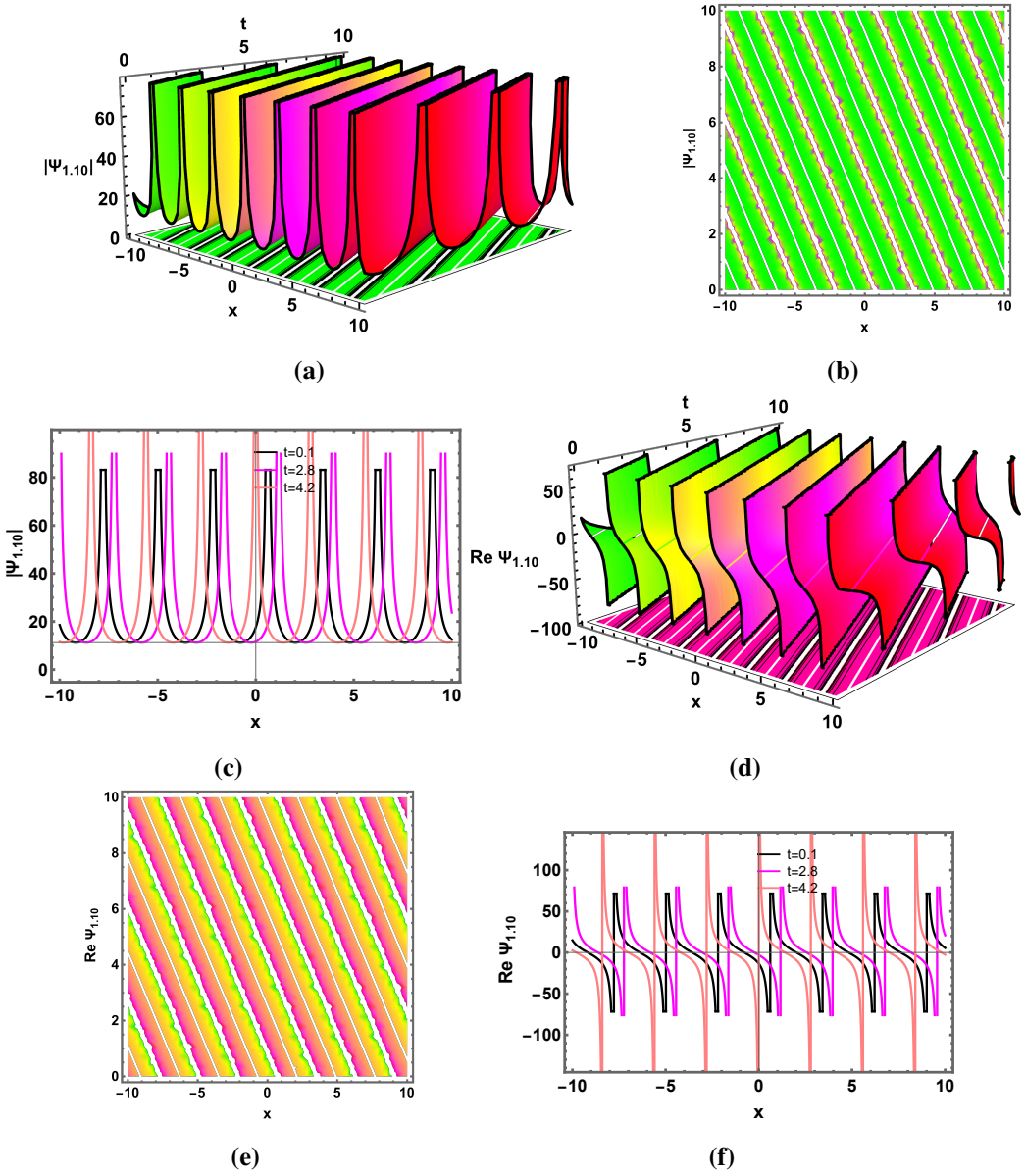

Figure 8. Dynamics of periodic waves of solution (3.18) for the parameters $\varpi = 3.5$, $W_{x,1} = 0.6$, $W_{t,1} = 0.5$, and $G = 0.2$.

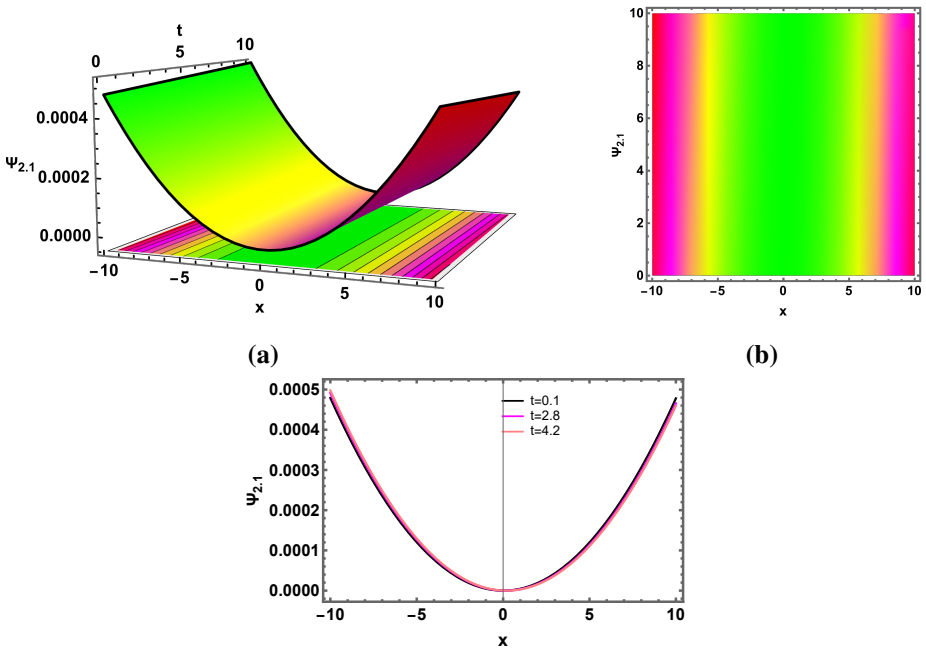

Figure 9. Dynamics of the dark soliton solution (3.24) for the parameters $\varpi = -0.02$, $W_{2,4} = 2$, $W_{4,\Psi} = 1.2$, $\gamma = 0.3$, $\alpha = 2.3$, and $W_{x,2} = 0.05$.

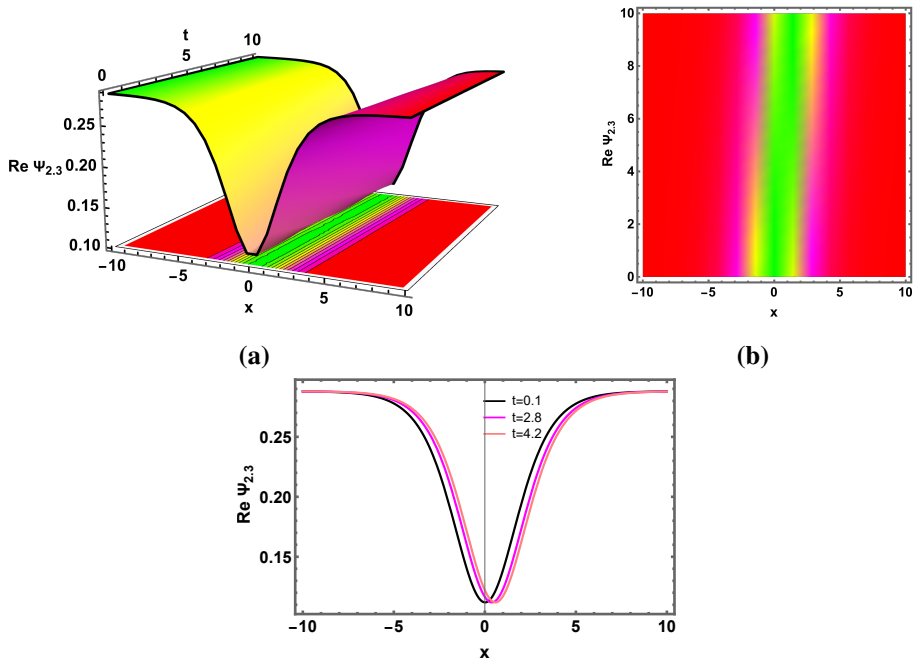

Figure 10. Dynamics of the real part of the solution (3.26) for the parameters $\varpi = -0.01$, $W_{2,4} = 2$, $W_{4,\Psi} = 2.2$, $\gamma = 1.3$, $\alpha = 0.03$, $W_{x,2} = 2.1$, and $b = .1$.

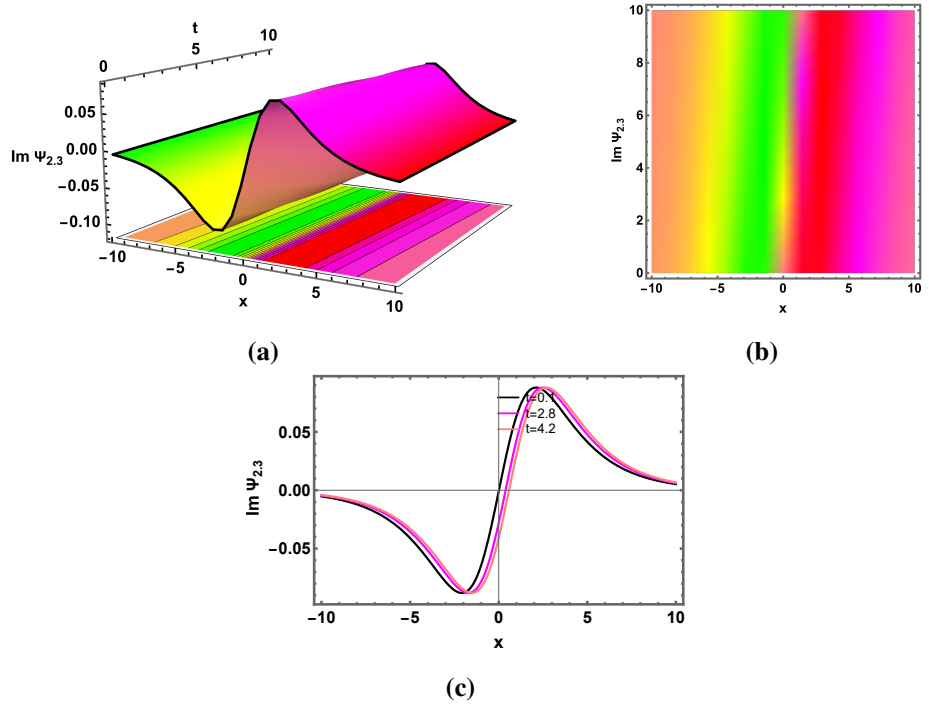

Figure 11. Dynamics of the imaginary part of the solution (3.26) for the parameters $\varpi = -0.01, W_{2,4} = 2, W_{4,\Psi} = 2.2, \gamma = 1.3, \alpha = 0.03, W_{x,2} = 2.1$, and $b = .1$.

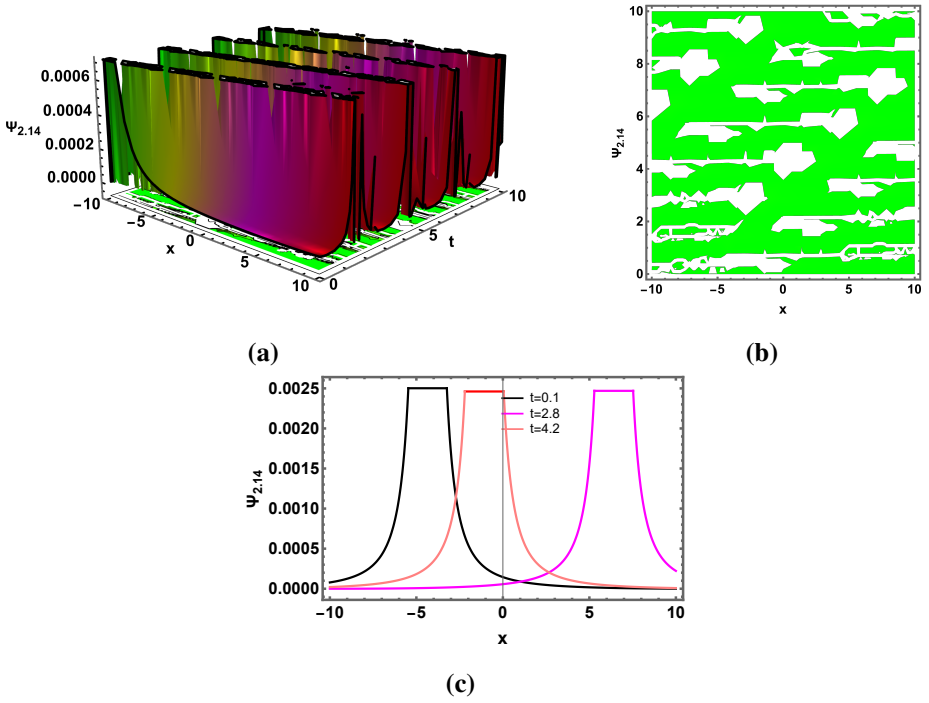

Figure 12. Dynamics of periodic waves of solution (3.37) for the parameters $\varpi = 0.06, W_{x,1} = 0.5, W_{2,4} = 0.2, W_{4,\Psi} = 0.002, \gamma = 3, \alpha = 0.3, W_{1,4} = 0.5, \chi = .2$, and $\varrho = 0.1$.

5. Concluding remarks

In conclusion, this work introduces a novel approach known as RSENNs for computing analytical solutions of complex PDEs. By means of the forward propagation of the NNs model, we are able to acquire the trial functions by inserting the solutions of the Riccati equation into the first hidden layer of the model. Each term's coefficients are combined and adjusted to zero using trial functions. The coefficients are found in an algebraic equation system using this procedure. These coefficients may be found by solving these algebraic equations. To get novel exact solutions, this innovative approach combines the traditional Riccati subequation method with the recently developing field of machine learning, helping to study complex mathematical and physical problems. Investigating the exact solutions of the nonlinear Murray equation and the nano-ionic currents along MTs dynamic equations has enabled us to confirm the applicability and adaptability of RSENNs to finding the exact solutions of NLPDEs. A comparison between studied method and other analytical methods have been provided in the Table 1. Researchers may use these equations to examine events related to nonlinear propagation. New exact solutions found in this work may serve as additional guidelines for future studies in this field. Analyzing wave dynamics via multidimensional plots (3D, 2D, contour, and density) can clarify complex mathematical and physical interactions in solutions.

Table 1. Comparison between RSENN and traditional analytical methods.

Method	ODE Conversion	Non-integrable PDEs	Solves PDEs Directly	Needs Balance Number
RSENN	No	Yes	Yes	No
Tanh Method	Yes	Limited	No	Yes
SEM	Yes	Limited	No	Yes

Author contributions

Jan Muhammad: Conceptualization, validation, investigation, writing the original draft; Ghulam Hussain Tipu: Methodology, software, writing-review and editing, visualization; Yasser Alrashedi: Validation, investigation, formal analysis, graphics; Mofareh Alhazmi: Writing-review and editing, software, methodology; Usman Younas: Supervision, validation, writing the original draft. All authors have read and agreed to the final version of the manuscript.

Use of Generative-AI tools declaration

The authors declare they have not used artificial intelligence (AI) tools in the creation of this article.

Conflict of interest

The authors declare no conflict of interest.

References

1. I. Alraddadi, F. Alsharif, S. Malik, H. Ahmad, T. Radwan, K. K. Ahmed, Innovative soliton

solutions for a (2+1)-dimensional generalized KdV equation using two effective approaches, *AIMS Math.*, **9** (2024), 34966–34980. https://doi.org/10.3934/math.20241664

2. J. Muhammad, U. Younas, Wave propagation and multistability analysis to the modified fractional KDV-KP equation in diversity of fields, *Model. Earth Syst. Env.*, **11** (2025), 262. https://doi.org/10.1007/s40808-025-02434-8

3. U. Demirbilek, A. H. Tedjani, A. R. Seadawy, Analytical solutions of the combined Kairat-II-X equation: A dynamical perspective on bifurcation, chaos, energy, and sensitivity, *AIMS Math.*, **10** (2025), 13664–13691. https://doi.org/10.3934/math.2025615

4. U. Younas, J. Muhammad, M. A. Murad, D. K. Almutairi, A. Khan, T. Abdeljawad, Investigating the truncated fractional telegraph equation in engineering: Solitary wave solutions, chaotic and sensitivity analysis, *Results Eng.*, **25** (2025), 104489. https://doi.org/10.1016/j.rineng.2025.104489

5. C. L. Fefferman, J. C. Robinson, J. L. R. Diez, J. L. Rodrigo, *Partial differential equations in fluid mechanics*, Cambridge University Press, 2018.

6. U. Demirbilek, Analytical study on the generalized q-deformed Sinh-Gordon (Eleuch) equation, *Comp. Math. Math. Phys.*, **65** (2025), 825–839. https://doi.org/10.1134/S0965542525700198

7. U. Younas, J. Muhammad, Q. Ali, M. Sediqmal, K. Kedzia, A. Z. Jan, On the study of solitary wave dynamics and interaction phenomena in the ultrasound imaging modelled by the fractional nonlinear system, *Sci. Rep.*, **14** (2024), 26080. https://doi.org/10.1038/s41598-024-75494-y

8. M. Kumar, Umesh, Recent development of Adomian decomposition method for ordinary and partial differential equations, *Int. J. Appl. Comput. Math.*, **8** (2022), 81. https://doi.org/10.1007/s40819-022-01285-6

9. N. Raza, B. Rani, Y. Chahlaoui, N. A. Shah, A variety of new rogue wave patterns for three coupled nonlinear Maccari's models in complex form, *Nonlinear Dynam.*, **111** (2023), 18419–18437. https://doi.org/10.1007/s11071-023-08839-3

10. N. Raza, F. Salman, A. R. Butt, M. L. Gandarias, Lie symmetry analysis, soliton solutions and qualitative analysis concerning to the generalized q-deformed Sinh-Gordon equation, *Commun. Nonlinear Sci.*, **116** (2023), 106824. https://doi.org/10.1016/j.cnsns.2022.106824

11. M. Ajmal, J. Muhammad, U. Younas, E. Hussian, M. El-Meligy, M. Sharaf, Exploring the Gross-Pitaevskii model in Bose-Einstein condensates and communication systems: Features of solitary waves and dynamical analysis, *Int. J. Theor. Phys.*, **64** (2025), 64. https://doi.org/10.1007/s10773-025-05937-3

12. S. D. Zhu, The generalizing Riccati equation mapping method in non-linear evolution equation: Application to (2+1)-dimensional Boiti-Leon-Pempinelle equation, *Chaos Soliton. Fract.*, **37** (2008), 1335–1342. https://doi.org/10.1016/j.chaos.2006.10.015

13. M. Manas, Darboux transformations for the nonlinear Schrödinger equations, *J. Phys. A-Math. Gen.*, **29** (1996), 7721. https://doi.org/10.1088/0305-4470/29/23/029

14. K. Hosseini, F. Samadani, D. Kumar, M. Faridi, New optical solitons of cubic-quartic nonlinear Schrödinger equation, *Optik*, **157** (2018), 1101–1105. https://doi.org/10.1016/j.ijleo.2017.11.124

15. J. Muhammad, Q. Ali, U. Younas, On the analysis of optical pulses to the fractional extended nonlinear system with mechanism of third-order dispersion arising in fiber optics, *Opt. Quant. Electron.*, **56** (2024), 1168. https://doi.org/10.1007/s11082-024-07061-8

16. U. Younas, E. Hussain, J. Muhammad, M. Sharaf, M. E. Meligy, Chaotic structure, sensitivity analysis and dynamics of solitons to the nonlinear fractional longitudinal wave equation, *Int. J. Theor. Phys.*, **64** (2025), 42. https://doi.org/10.1007/s10773-025-05916-8

17. T. Han, Z. Li, C. Li, Bifurcation analysis, stationary optical solitons and exact solutions for generalized nonlinear Schrödinger equation with nonlinear chromatic dispersion and quintuple power-law of refractive index in optical fibers, *Physica A*, **615** (2023), 128599. https://doi.org/10.1016/j.physa.2023.128599

18. J. Wang, Y. Liu, L. Yan, K. Han, L. Feng, R. Zhang, Fractional sub-equation neural networks (fSENNs) method for exact solutions of space-time fractional partial differential equations, *Chaos: An Interd. J. Nonlinear Sci.*, **35** (2025), 043110. https://doi.org/10.1063/5.0259937

19. J. Zhuang, P. Meng, W. Yin, A stable neural network for inverse scattering problems with contaminated data, *Knowl.-Based Syst.*, **310** (2025), 113001. https://doi.org/10.1016/j.knosys.2025.113001

20. R. Yang, P. J. Schmid, Complex-network modeling of reversal events in two-dimensional turbulent thermal convection, *J. Fluid Mech.*, **1011** (2025), A30. https://doi.org/10.1017/jfm.2025.371

21. P. Meng, X. Wang, W. Yin, ODE-RU: A dynamical system view on recurrent neural networks, *Electron. Res. Arch.*, **30** (2022), 257–271. https://doi.org/10.3934/era.2022014

22. S. Phoosree, N. Khongnual, J. Sanjun, A. Kammanee, W. Thadee, Riccati sub-equation method for solving fractional flood wave equation and fractional plasma physics equation, *Part. Differ. Equ. Appl. Math.*, **10** (2024), 100672. https://doi.org/10.1016/j.padiff.2024.100672

23. E. S. Al-Rawi, A. F. Qasem, Numerical solution for nonlinear murray equation using the operational matrices of the Haar wavelets method, *Tikrit J. Pure Sci.*, **15** (2010), 288–294.

24. R. M. Cherniha, New ansätze and exact solutions for nonlinear reaction-diffusion equations arising in mathematical biology, *Symmetry Nonlinear Math. Phys.*, **1** (1997), 138–146.

25. M. Inc, S. Hussain, A. H. Ali, M. S. Iqbal, R. Ashraf, M. A. Tarar, et al., Analyzing solitary wave solutions of the nonlinear Murray equation for blood flow in vessels with non-uniform wall properties, *Sci. Rep.*, **14** (2024), 10588. https://doi.org/10.1038/s41598-024-61276-z

26. S. Kumbinarasaiah, M. Mulimani, A study on the non-linear murray equation through the bernoulli wavelet approach, *Int. J. Appl. Comput. Math.*, **9** (2023), 40. https://doi.org/10.1007/s40819-023-01500-y

27. T. Mitchison, M. Kirschner, Microtubule assembly nucleated by isolated centrosomes, *Nature*, **312** (1984), 232–237. https://doi.org/10.1038/312232a0

28. M. Kirschner, T. Mitchison, Beyond self-assembly: From microtubules to morphogenesis, *Cell*, **45** (1986), 329–342. https://doi.org/10.1016/0092-8674(86)90318-1

29. N. H. Aljahdaly, A. F. Alyoubi, A. R. Seadawy, Solitary wave solutions of the ionic currents along microtubule dynamical equations via analytical mathematical method, *Open Phys.*, **19** (2021), 494–503. https://doi.org/10.1515/phys-2021-0059

30. W. R. Juadih, M. Candan, G. Singh, B. Eslami, J. Manafian, I. Kaur, et al., On traveling wave solutions for the transmission line model of nano-ionic currents along MTs arising in nanobiosciences, *Opt. Quant. Electron.*, **56** (2024), 635. https://doi.org/10.1007/s11082-024-06277-y

AIMS Press